A Fuzzy - Based Framework for Assessing Uncertainty in Drift Prediction Using Observed Currents and Winds

1 SUPPLEMENTARY DATA

1.1 Fuzzy Numbers - Hypothetical Example

It is of interest to predict the drift speed of a ship that has lost power at sea during a winter storm, with the only available information being forecast wind speeds. From the literature, one might reasonably conclude that the ship will drift at 3% of the wind speed and this value is therefore assigned a state of 'certainly possible' and a membership of 1. However it is also known that the forecast wind speeds are generally within 10% of the true value. Therefore we can say that ship drift at a rate between 2.7% and 3.3% of the wind speed is 'likely possible' and assign this range a membership of 0.7, or a similar value below 1 that is representative of the likelihood of error due to inaccurate wind forecasts. Further, it is known that strong surface stratification may increase the ship's drift speed by up to 2% of the wind speed. The ship's location is relatively far from significant freshwater inflows and given the winter season diurnal heating is considered to be unlikely to produce sufficient stratification to increase drift speed. However no information is available to rule out this scenario, and therefore we consider the range of ship drift between 2.7% and 5.3% of the wind speed to be 'maybe possible' and assign it a membership of 0.4. Finally, we are confident that none of our assumptions are in error by more than 20% and therefore we set the range 2.16% to 6.36% as our lowest membership level, with membership zero. Values outside this range are considered to be 'impossible'. The resulting membership function of the fuzzy number describing ship drift as a percentage of wind speed is shown in Figure S8.

1.2 Comparison of Current Meter and ADCP at Ocean Station Papa

To investigate potential differences in the measurements recorded by the single point current meter and the ADCP at Ocean Station Papa we plot the vector correlation between the current meter record and the ADCP record at all available depths, following Kundu (1976). The vector correlation is expressed as,

$$R = \frac{< w^{`*}_{CM} w^{`}_{ADCP} >}{\sqrt{< w^{`*}_{CM} w^{`}_{CM} >< w^{`*}_{ADCP} w^{`}_{ADCP} >}} \tag{S1}$$

where $w^{`}_{CM/ADCP}$ are the detrended recorded velocities expressed as a complex number $w = u + iv$. The superscript $*$ denotes the complex conjugate, and $<>$ denotes an ensemble average. From R we can obtain the magnitude of the correlation, $|R|$, as well as the mean angle between the vectors, $Phase(R)$. These are plotted in Figure S9 for the raw current meter record as well as the current meter smoothed to 30 minute intervals using a boxcar filter.

Clearly the measurements are well correlated throughout the measurement depth of the ADCP (up to ~70 m) and peaking near the depth of the current meter, however relative flow direction changes throughout the water column by $\pm$ ~10° as would be expected in wind-driven Ekman-type flow. Smoothing the current meter data does not change these results appreciably. Comparing the timeseries of the current meter record

and the 6 m ADCP bin during the first seven days of the drifter deployment visually confirms this strong correlation (Figure S10).

However the ADCP data does not indicate significant persistent vertical structure in the magnitude of the currents, as indicated by the time-averaged profile of the ADCP data over the course of the simulation considered in the main paper. The proposed model for vertical shear (Equation 9 of the main paper) shows strong surface intensification. The shear below the surface is relatively consistent with the ADCP, though slightly higher in the northward direction by $\sim$2 cm/s (Figure S11).

The correlation between the current meter and the ADCP data also tracks the depth profile of good data returned relatively well (Figure S12). Data return increases from $\sim$85% in the bins closest to the surface to $\sim$100% by about 35 m depth. The largest number of bins with no good data are also clustered near the surface. Therefore it is not completely clear whether the ADCP captures an Ekman-like flow near the ocean surface or whether this is an artifact of comparatively sparse data return and significant spiking in the near-surface ADCP data.

In general, the ADCP record shows significantly more high-frequency spiking than the current meter record. The low-frequency signals match well, however the ADCP appears to report a lower amplitude of low-frequency signals at some times. This is similar to the comparison between the current meter and the 16 m bin of the ADCP, shown in Figure 1 of the main paper. To further investigate these differences we plot the distribution of the difference in measurements that are co-located in time in u, v space (Figures S13 & S14).

These distributions indicate that there is a significant ($\sim$3.2 cms^{-1}) bias between the two instruments, with mean current meter results directed more northeasterly than ADCP results ($E[u_{CM} - u_{ADCP}] > 0$, and $E[v_{CM} - v_{ADCP}] > 0$). This suggests that the mean flow recorded by the current meter is approximately opposite to the much smaller mean flow recorded by the ADCP at a shallower depth. The differences approximately follow a Gaussian distribution with this mean, with the standard deviation being indicative of energy at time scales that are not resolved by the ADCP as well as the spiking noted earlier. The difference noted here is consistent with the difference between the shear recorded by the ADCP and the values estimated by Equation 9, as noted above.

Plotting a similar diagram comparing the current meter record with the closest ADCP bin (16 m) shows that the northwesterly bias of the current meter with respect to the ADCP persists at this depth and increases in magnitude to $\sim$ 4.1 cms^{-1}, which suggests that this is a systematic discrepancy between the two instruments rather than a feature of the near-surface current dynamics. The distribution of discrepancies at this depth is significantly more peaked than a Gaussian distribution, which is again consistent with periodic spiking.

REFERENCES

Dagestad, K.-F., Röhrs, J., Breivik, Ø., and Ådlandsvik, B. (2018). Opendrift v1.0: a generic framework for trajectory modelling. *Geoscientific Model Development* 11, 1405–1420. doi:10.5194/gmd-11-1405-2018

Kundu, P. K. (1976). Ekman veering observed near the ocean bottom. *Journal of Physical Oceanography* 6, 238–242. doi:10.1175/1520-0485(1976)006⟨0238:EVONTO⟩2.0.CO;2

Lellouche, J.-M., Greiner, E., Bourdallé-Badie, R., Garric, G., Melet, A., Drévillon, M., et al. (2021). The Copernicus global 1/12 oceanic and sea ice GLORYS12 reanalysis. *Frontiers in Earth Science* 9

2 SUPPLEMENTARY TABLES AND FIGURES

2.1 Figures

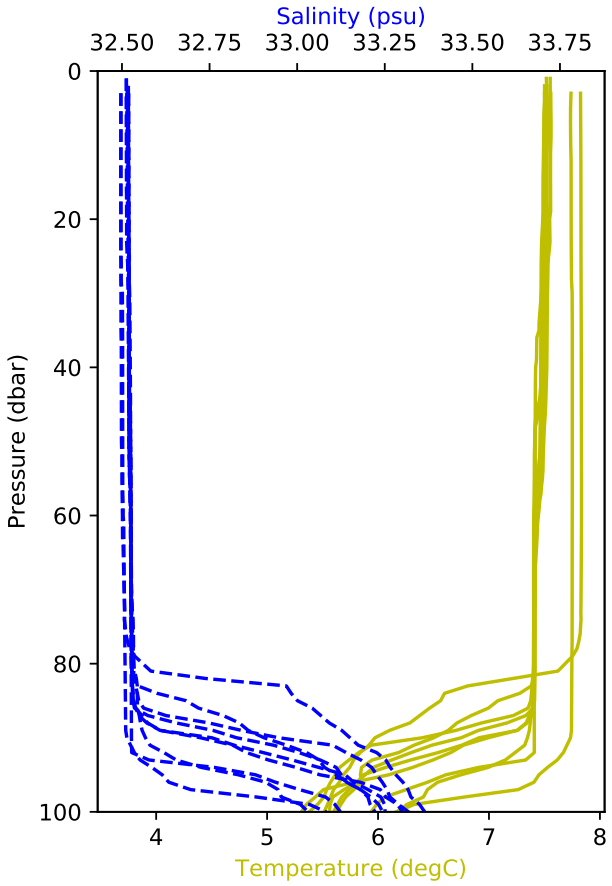

Figure S1. Profiles of temperature (yellow) and salinity (dashed blue) taken between Feb 18 - 19, 2015. Data is available at www.waterproperties.ca.

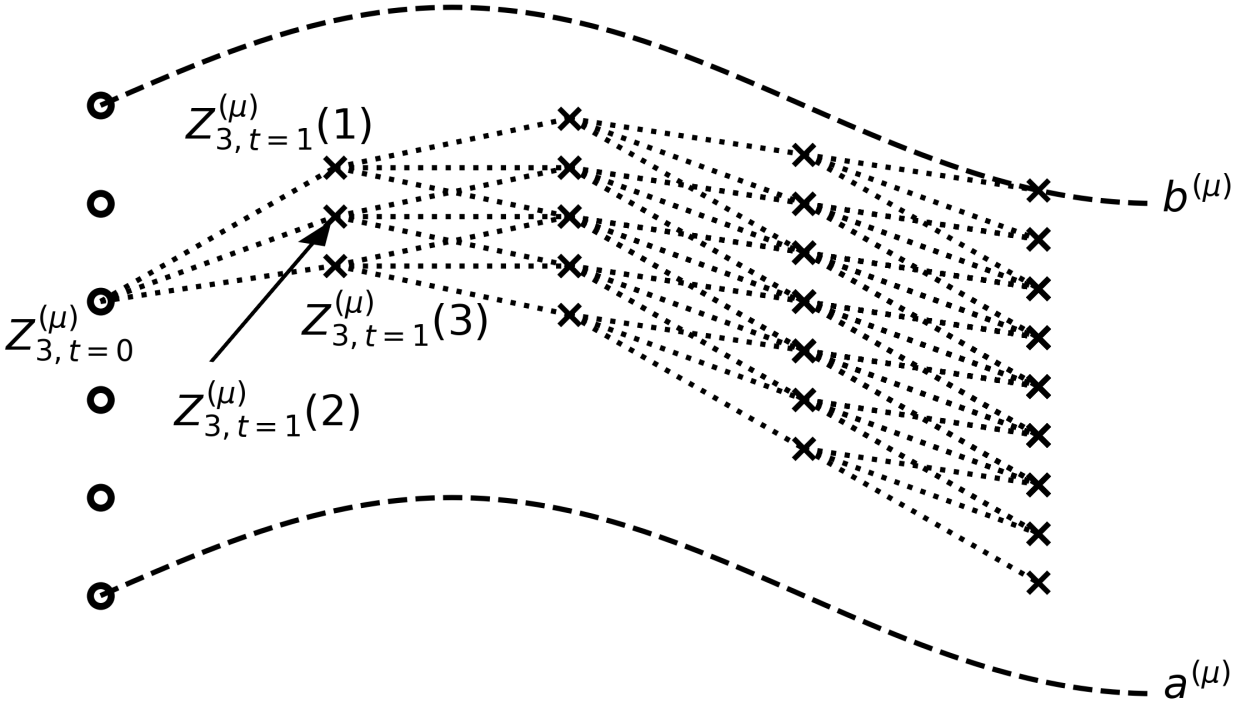

Figure S2. Illustration of the scheme to derive all possible crisp time series corresponding to a fuzzy time series of drift velocity. An example of the first four time steps starting from point $m = 3$ with $n_p = 3$ is shown here.

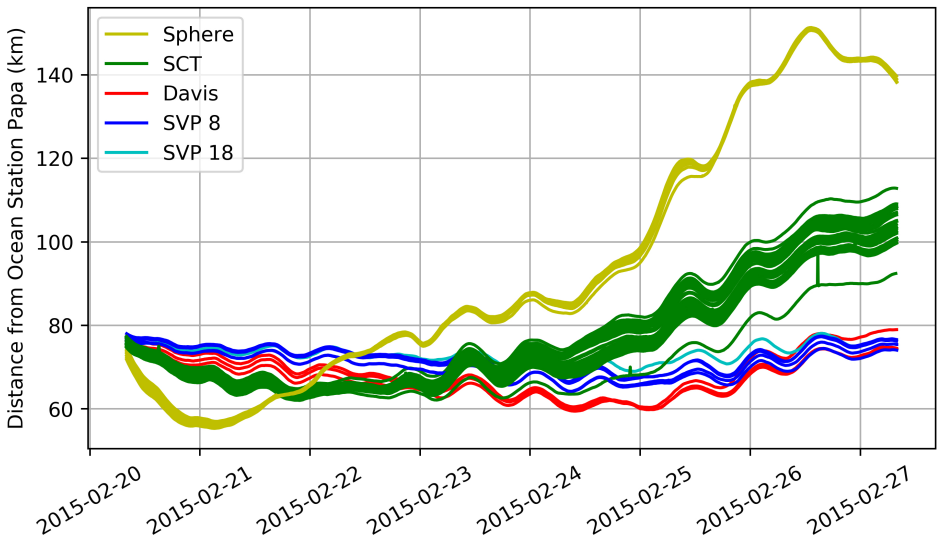

Figure S3. Distance of drifters from Ocean Station Papa during the first seven days of the deployment.

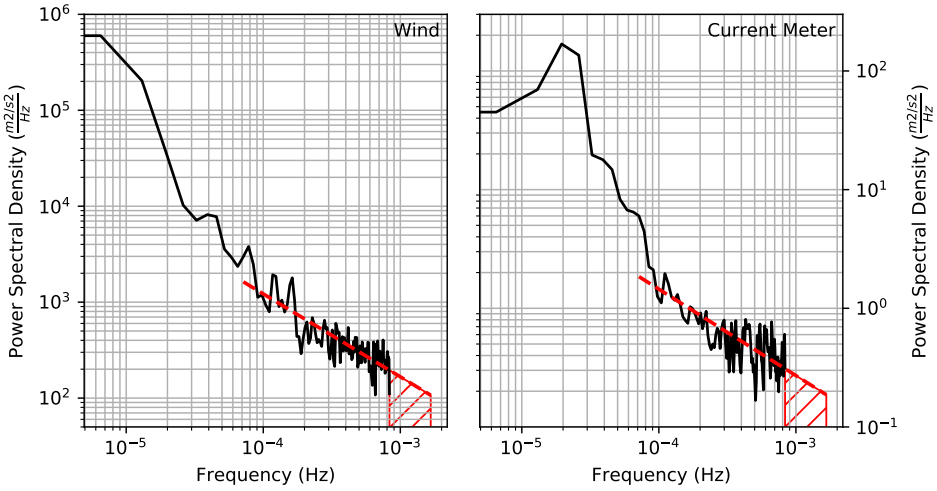

Figure S4. Power spectra of measured wind (left) and current (right). Power law fit to the high-frequency tail is shown in dashed red and the area corresponding to the energy in unresolved timescales is hatched in red.

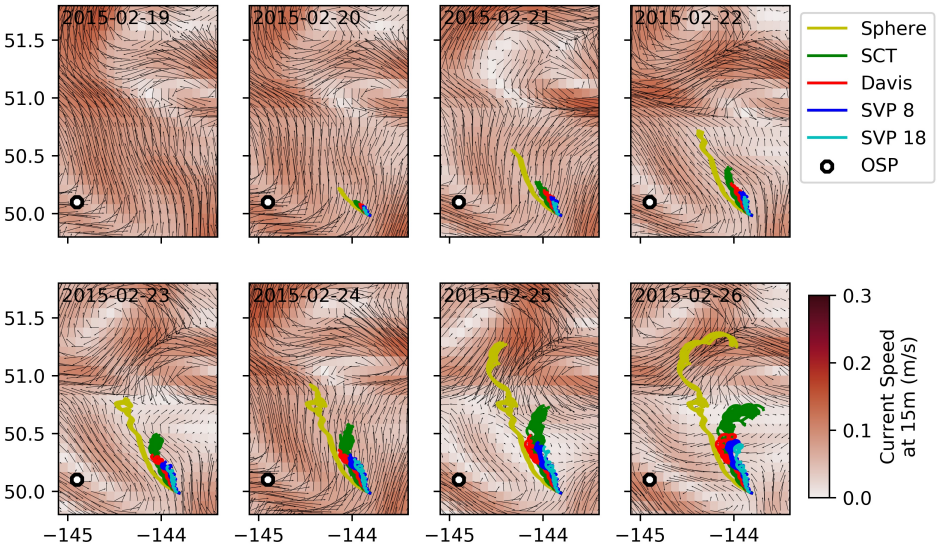

Figure S5. Daily-mean currents in the study area at 15 m depth from the GLORYS12 numerical re-analysis for Feb 19 - 26, 2015 (Lellouche et al., 2021). Data is available at `resources.marine.copernicus.eu/product-detail/GLOBAL_REANALYSIS_PHY_001_030/INFORMATION`.

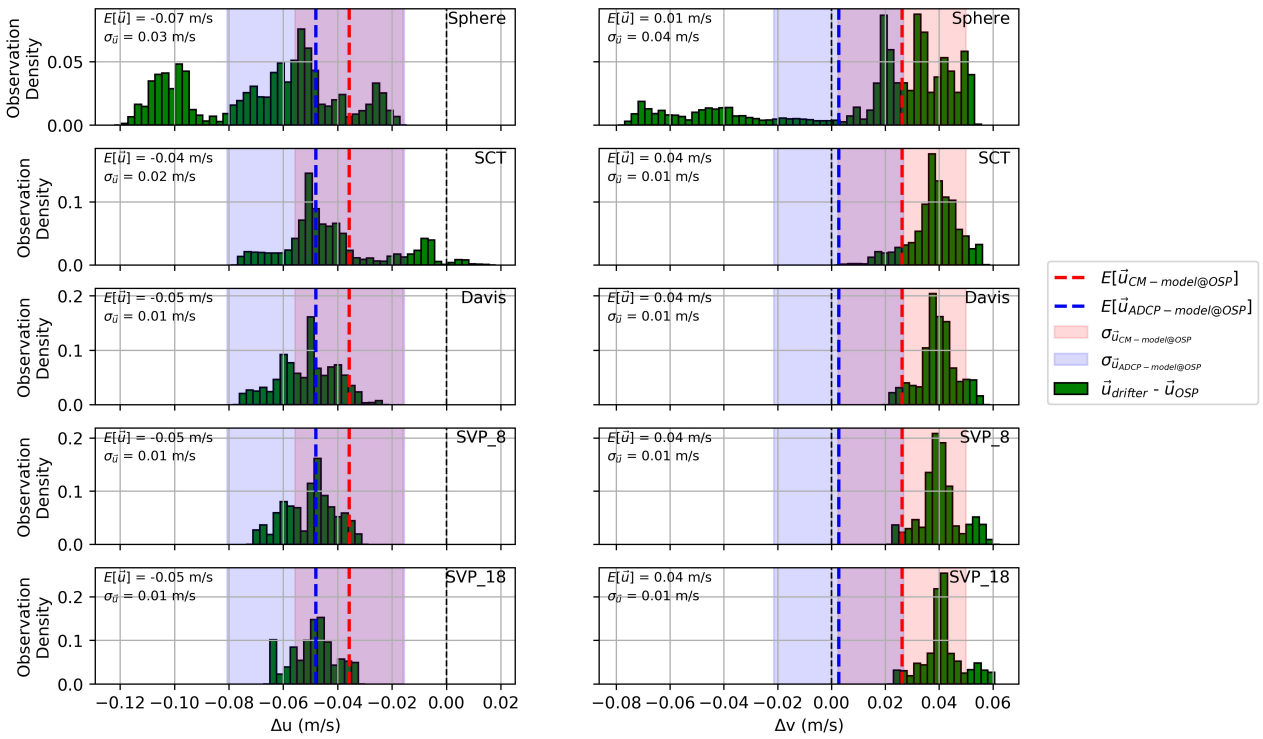

Figure S6. Differences in the daily-mean currents from GLORYS12 between OSP and the locations of the drifters. Each row represents values for a drifter type, with u-components (E-W, east positive) on the left and v components (N-S, north positive) on the right. The differences between modelled and observed currents are shown for the observations from the current meter (red) and the ADCP (blue). Mean differences are shown by the dashed line while the shading represents one standard deviation.

Table S1. Leeway coefficients for proxy object types for drifters used in this study. Reproduced from the OpenDrift source code (Dagestad et al., 2018) found at `github.com/OpenDrift/opendrift/blob/master/opendrift/models/OBJECTPROP.DAT`.

	Bait Box, lightly loaded	**WW2 Mine**	**Oil Drum**	**PIW, vertical**
Downwind Slope (%)	2.53	1.07	0.75	0.48
Downwind Offset (%)	9.01	4.47	2.66	0.00
Downwind Std. Dev. (%)	3.05	6.55	2.83	8.30
Right-crosswind Slope (%)	1.09	0.41	0.48	0.15
Right-crosswind Offset (%)	-2.76	1.15	2.88	0.00
Right-crosswind Std. Dev. (%)	4.14	4.13	3.92	6.70
Left-crosswind Slope (%)	-1.09	-0.41	-0.45	-0.15
Left-crosswind Offset (%)	2.76	-1.15	-1.46	0.00
Left-crosswind Std. Dev. (%)	4.14	4.13	4.59	6.70

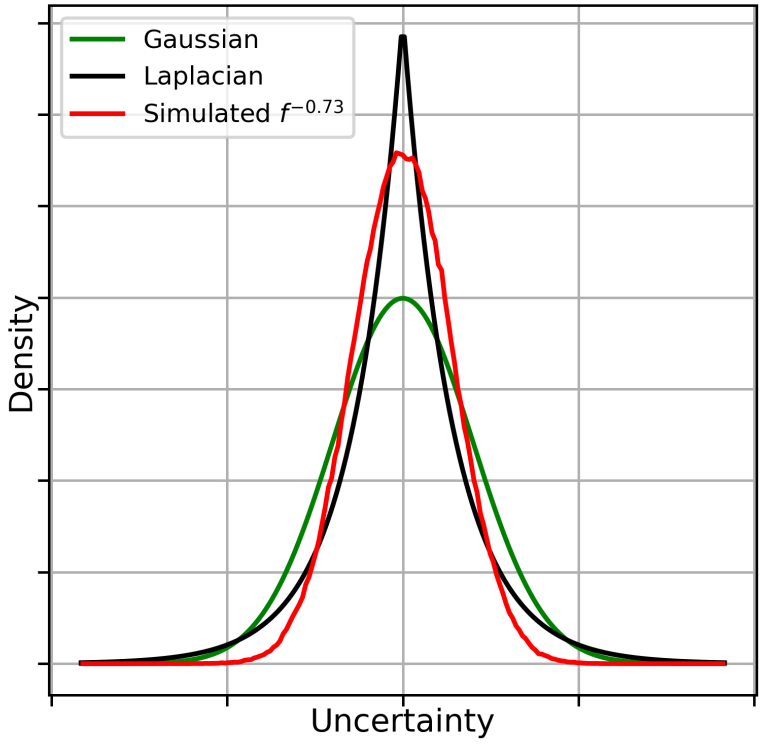

Figure S7. Generalized comparison of Gaussian and Laplace distributions with a simulated distribution from a red noise process with $f^{-\frac{3}{4}}$.

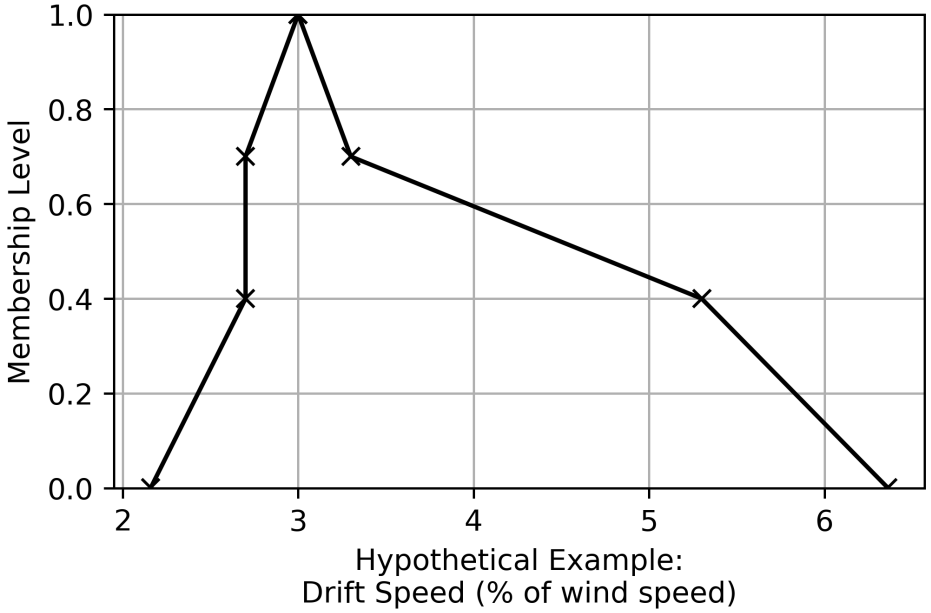

Figure S8. Membership function derived as hypothetical example in Section 3.1, for illustrative purposes only.

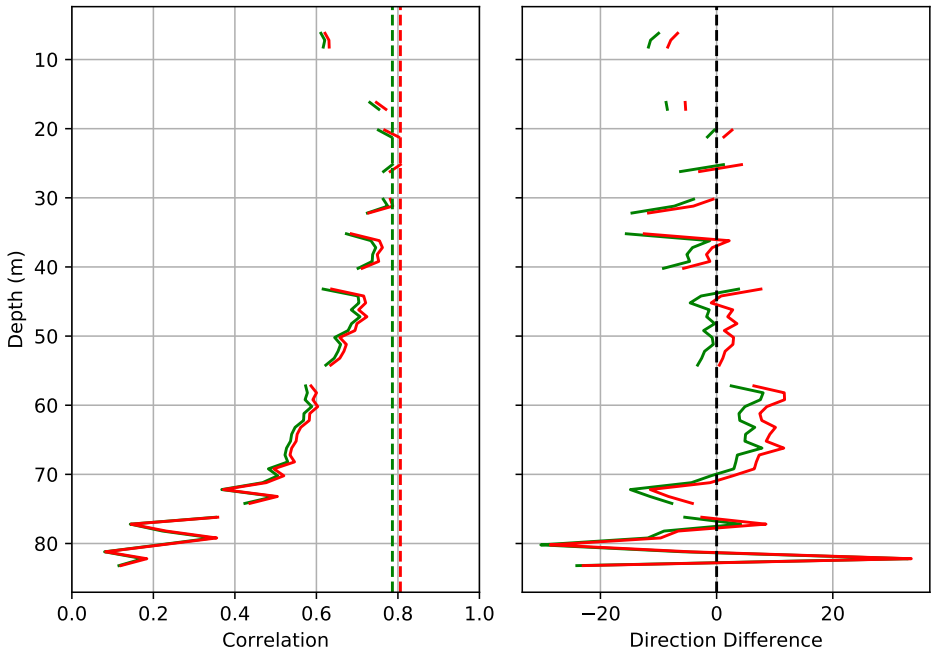

Figure S9. Magnitude (left) and phase (right) of the vector correlation between the ADCP record at all available depths and the current meter record at 15 m. Red lines indicate correlation with the raw current meter record, while green lines indicate correlations with the smoothed current meter record.

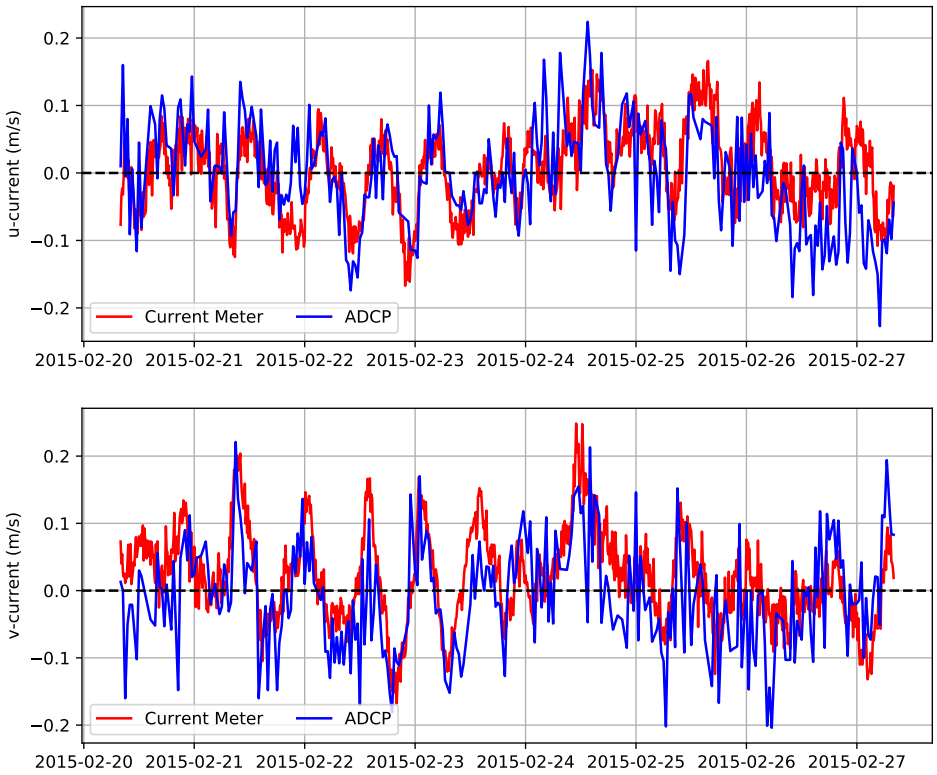

Figure S10. Timeseries of currents recorded by the current meter at 15 m depth (red) and the ADCP at 6 m depth (blue). u components (E-W) are shown on top and v components (N-S) below.

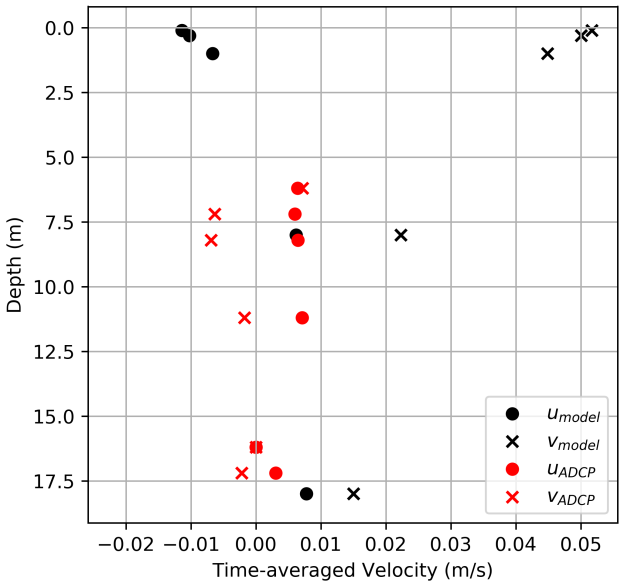

Figure S11. Time-averaged profile of velocity components from the ADCP, and the model for current shear (Equation 9) over the course of the simulation.

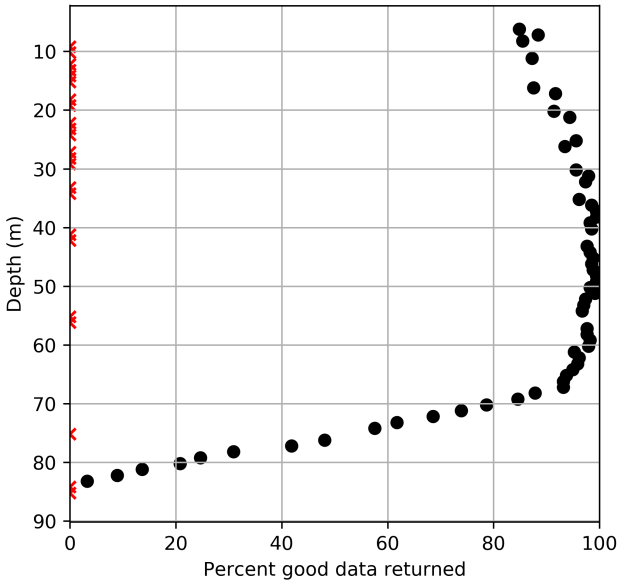

Figure S12. Depth profile of data return for the ADCP after quality control flags are applied. Bins with no good data are marked by red x's on the y-axis.

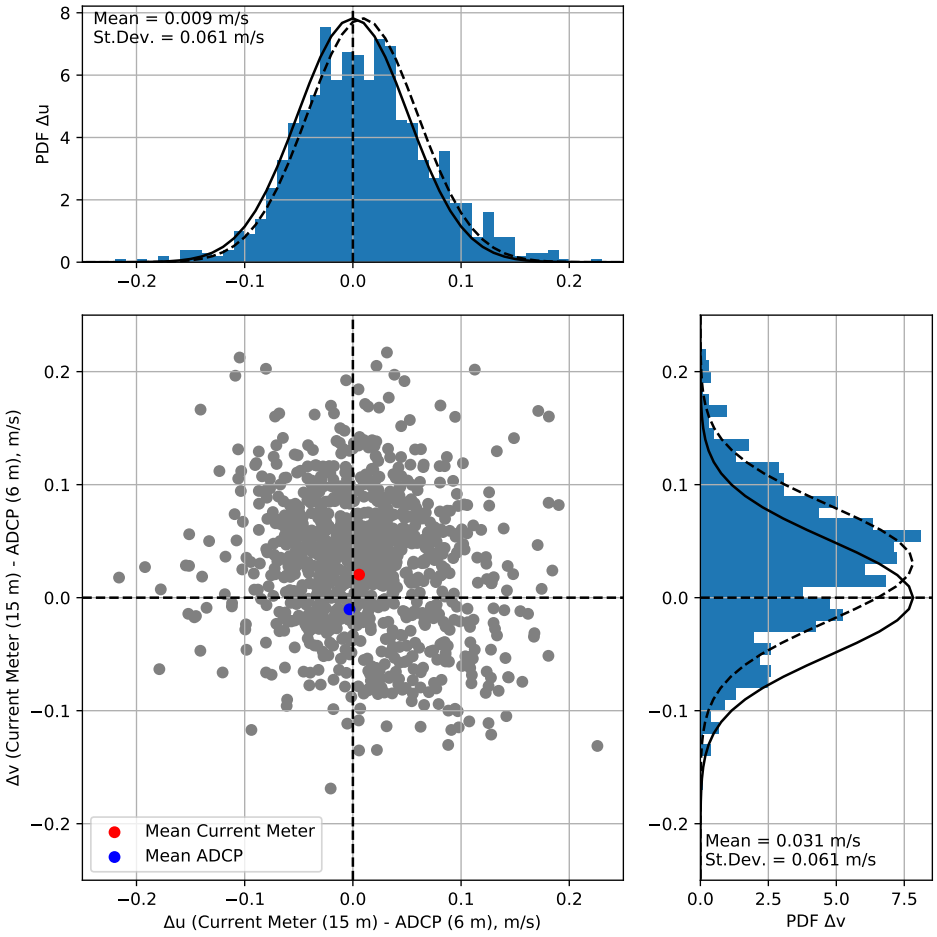

Figure S13. Difference between current meter at 15 m and ADCP measurements at 6 m, in u,v space. Distributions of component differences are shown in the side panels, with a Gaussian distribution superimposed. The solid line indicates a zero-mean distribution while the dotted line indicates a distribution that is shifted to the bias between the two data sources. The time-averaged currents recorded by the current meter and the ADCP are shown by the colored markers.

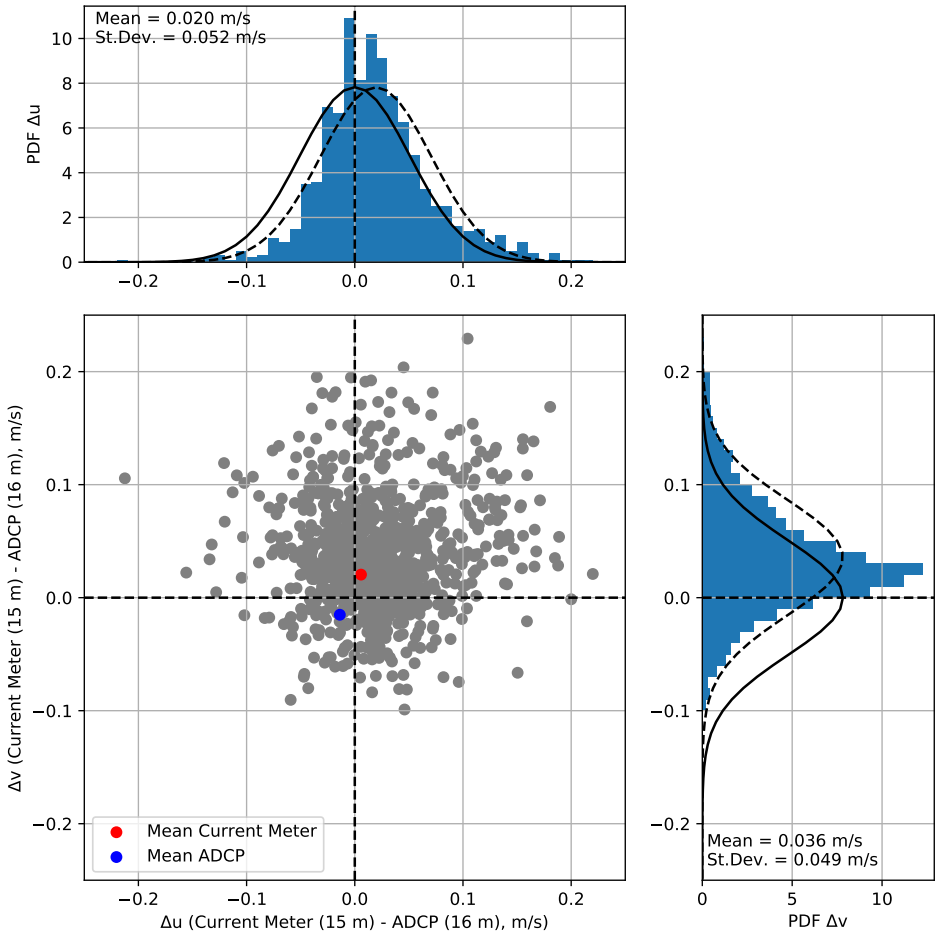

Figure S14. Same as Figure S13, but for ADCP bin at 16m.